Available online at www.sciencedirect.com

ScienceDirect

journal homepage: www.elsevier.com/locate/he

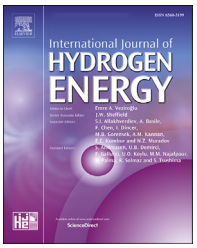

Plasma-catalytic ammonia decomposition using a packed-bed dielectric barrier discharge reactor

J.A. Andersen [a], J.M. Christensen [a], M. Østberg [b], A. Bogaerts [c], A.D. Jensen [a,*]

[a] Department of Chemical and Biochemical Engineering, Technical University of Denmark, 2800, Kgs. Lyngby, Denmark

[b] Haldor Topsøe A/S, Haldor Topsøes Allé 1, 2800, Kgs. Lyngby, Denmark

[c] Research Group PLASMANT, Department of Chemistry, University of Antwerp, 2610, Wilrijk, Belgium

HIGHLIGHTS

- The plasma was found to achieve an NH_3 conversion of 5% at ambient conditions.
- Introduction of dielectric materials with $\varepsilon = 4–30$ improved conversion.
- $MgAl_2O_4$ ($\varepsilon = 8.3$) yielded the highest conversion found of 15%.
- A linear correlation between conversion and number of micro-discharges was found.
- The decomposition primarily proceeds in the gas phase by collision with electrons.

ARTICLE INFO

Article history:
Received 14 July 2021
Received in revised form
7 July 2022
Accepted 12 July 2022
Available online 17 August 2022

Keywords:
Ammonia decomposition
Clean hydrogen
Plasma catalysis
DBD Plasma

ABSTRACT

Plasma-catalytic ammonia decomposition as a method for producing hydrogen was studied in a packed-bed dielectric barrier discharge (DBD) reactor at ambient pressure and a fixed plasma power. The influence of packing the plasma zone with various dielectric materials, typically used as catalyst supports, was examined. At conditions (21 W, 75 Nml/min NH_3) where an NH_3 conversion of 5% was achieved with plasma alone, an improved decomposition was found when introducing dielectric materials with dielectric constants between 4 and 30. Of the tested materials, $MgAl_2O_4$ yielded the highest conversion (15.1%). The particle size (0.3–1.4 mm) of the $MgAl_2O_4$ packing was found to have a modest influence on the conversion, which dropped from 15.1% to 12.6% with increasing particle size. Impregnation of $MgAl_2O_4$ with different metals was found to decrease the NH_3 conversion, with the Ni impregnation still showing an improved conversion (7%) compared to plasma-only. The plasma-assisted ammonia decomposition occurs in the gas phase due to micro-discharges, as evident from a linear correlation between the conversion and the frequency of micro-discharges for both plasma alone and with the various solid packing materials. The primary function of the solid is thus to facilitate the gas phase reaction by assisting the creation of micro-discharges. Lastly, insulation of the reactor to raise the temperature to 230 °C in the plasma zone was found to have a negative effect on the conversion, as a change from volume discharges to surface discharges occurred. The study shows that NH_3 can be decomposed to provide

* Corresponding author.
E-mail address: Aj@kt.dtu.dk (A.D. Jensen).

https://doi.org/10.1016/j.ijhydene.2022.07.102

hydrogen by exposure to a non-thermal plasma, but further developments are needed for it to become an energy efficient technology.

Introduction

Hydrogen (H_2) is considered an important fuel of the future, because it is a clean energy source with water as the only product from its combustion [1,2]. Certain small-scale power generation units, such as fuel cells, use H_2 as fuel for production of green electricity. However, delivery and storage of H_2 is hindering the commercialization of H_2 fuel cell-based processes, along with catalyst and reactor stability of a fuel cell system [3]. On-site H_2 generation via ammonia (NH_3) is currently investigated as a solution to the delivery and storage issue, because NH_3 can be condensed at room temperature (25 °C) and a relatively low pressure of ca. 10 atm, which yields a higher volumetric energy density than pressurized H_2 [3–6]. Furthermore, NH_3 decomposition in principle only yields nitrogen (N_2) as by-product (see Reaction 1).

$$2\,NH_3 \rightarrow 3\,H_2 + N_2 \quad , \quad \Delta_r H = 46.2\ kJ/mol \qquad R1$$

To use NH_3 as a H_2 carrier, effective conversion processes that avoid formation of byproducts, such as hydrazine [7], should be developed. Several heterogeneous catalysts, such as Ru, Ni, Fe, and Co, are capable of promoting the reaction, but require reaction temperatures above 500 °C to achieve a reasonable conversion level [8–14]. Lendzion-Bielun et al. [8] found that Co promoted with small amounts of Al_2O_3, CaO, and K_2O could reach an NH_3 conversion of 50%, while Li et al. [13] found that Ru/SiO_2 could achieve 96.5% conversion and Ni/SiO_2 only could reach 34.6%, all at 550 °C. Furthermore, Silva et al. [14] reached an NH_3 conversion of >99% with a Fe–Ni/γ-Al_2O_3 egg-shell catalyst at a temperature of 650 °C.

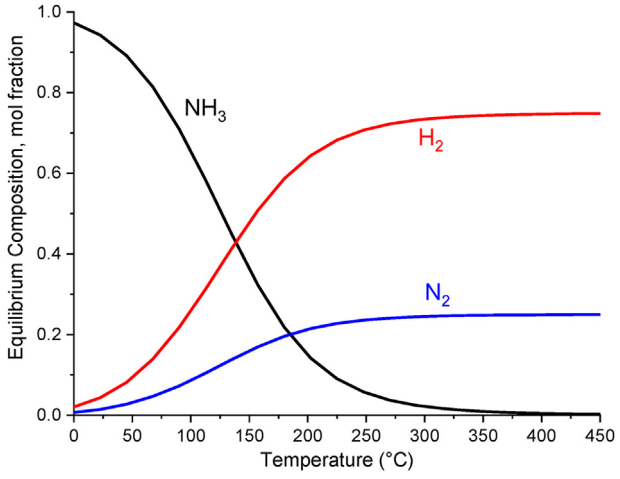

Fig. 1 – Equilibrium composition of NH_3, H_2, and N_2 as function of temperature at 1 atm.

However, the thermodynamic equilibrium (Fig. 1) shows that a conversion of >99% can be achieved at a temperature of 375 °C. Further development of inexpensive metal catalysts that can reach a reasonable conversion at lower temperatures, or alternative processes, are therefore required to improve the H_2 generation via NH_3 decomposition.

Recently, the use of plasma-catalytic processes have shown an enhanced ability for NH_3 decomposition where both diluted [15–17] and pure NH_3 feeds have been investigated [18–23]. Akiyama et al. [15] examined NH_3 decomposition in a DBD reactor with wool-like inner electrodes consisting of different metals (Ag, Al, Cu, Fe, and Ti) in a range of applied power. No external heating was used and the gas mixture contained 4.87% NH_3 in N_2 [15]. The decomposition rate was found to be independent of the electrode metal employed and linearly dependent on power in the range 0–50 W, with full decomposition achieved at approximately 50 W. El-Shafie et al. [16] investigated the effect of Al_2O_3 particle size (1–2 mm) with a 0.5% NH_3-Ar feed and found that the smaller particle size (1 mm) yielded a higher NH_3 conversion independent of feed flow rate (0.1–1 l/min) and plasma voltage (12–18 kV). In another study by El-Shafie et al. [17] the effect of using different packing materials (Ru/Al_2O_3 and SiO_2) was explored. Here an increased energy efficiency was reported when using Ru/Al_2O_3 compared to SiO_2 when operating with a plasma voltage of 18 kV. Wang et al. [21] found that when introducing a commercial Fe-based NH_3-synthesis catalyst in a DBD reactor at 410 °C, an NH_3 conversion of 99.9% could be achieved, while plasma alone and catalyst alone only reached 7.8% and 7.4% conversion, respectively. Hence, the plasma-catalytic system reached a conversion close to the thermodynamic limit (see Fig. 1). In another study, Wang et al. [20] showed that a Co/SiO_2 catalyst yielded an NH_3 conversion of 20% at 450 °C and in combination with plasma a conversion of 99.2% was obtained. In both studies, pure NH_3 gas at a flow rate of 40 ml/min was examined [20,21]. Hayakawa et al. [23] utilized a membrane DBD reactor to investigate the decomposition of NH_3, where the plasma zone was 30 cm long. In the study they found that the membrane reactor increased the H_2 rate by ca. 87% compared to a reactor without a membrane [23]. This indicates that an equilibrium can occur in the plasma and that removing H_2 will improve the NH_3 decomposition.

As evident from the few studies of plasma-driven NH_3 decomposition in the literature, only little is known about the influence of solid, potentially catalytic, packing materials in the plasma zone, and more fundamental research is needed. In this study, decomposition of NH_3 was studied and the influence of utilizing different dielectric materials (alone or impregnated with various metals) in the discharge zone were

examined. In addition, the fresh and spent catalysts were characterized using X-ray diffraction (XRD).

Experimental

Dielectric barrier discharge setup

A coaxial packed-bed DBD reactor of quartz was used for the plasma-catalytic ammonia decomposition as shown in Fig. 2. The outer electrode was a stainless steel mesh tightly wrapped around the reactor with a length of 5 cm, while the inner electrode was a stainless steel rod with an outer diameter of 10 mm. The inner diameter and wall thickness of the reactor were 19 mm and 1.5 mm, respectively, yielding a discharge gap of 4.5 mm and corresponding discharge volume of 10.2 cm^3. The outer electrode was connected to a high voltage amplifier (TREK, model 20/20C-HS), which was controlled by a function generator (Tektronix, AFG1022). A high voltage probe (Tektronix, P6015A) was connected to the outer electrode to measure the applied voltage, while a Rogowski coil (Pearson, 4100) measured the current on the grounded line. Moreover, a low voltage probe (Picotech TA150) was used to measure the generated charges (Q) over an external capacitor (10 nF) placed in series on the grounded line. A digital oscilloscope (Picotech, Picoscope 6402C) was used for continuous recording of voltage, current, and charges, and calculation of plasma power.

The decomposition of NH_3 was mostly carried out at a plasma power of 21 W and a frequency of 3.0 kHz, except for experiments utilizing KM1R and TiO_2 (see further below) as packing material. Here a maximal plasma power of only 15 W could be achieved due to limitations of the amplifier. Complete filling of the discharge volume with packing material was utilized for the plasma catalysis experiments, equivalent to ca. 10 cm^3 of material. Glass wool was placed outside of the discharge zone on each side of the bed to hold the catalytic material in place. All experiments were conducted at atmospheric pressure without external heating. A flow of N_2 was passed through the reactor for 10 min to remove any oxygen, after which an NH_3 feed flow (99.999% purity) was maintained for 20 min to remove the N_2 before ignition of the plasma. After plasma ignition, a period of 2 h was used to stabilize the plasma.

NH_3 was fed to the reactor at a flow rate of 75 Nml/min through a Bronkhorst mass flow controller and the effluent was bubbled through a dilute aqueous solution of sulfuric acid to remove unconverted NH_3. This solution was placed in a cooling bath and kept at a temperature of 4 °C to avoid heating from the acid/base reaction and limit evaporation of water. The remaining flow ($H_2 + N_2$) was measured on a flow meter (Gilian, Gilibrator 2, with a range of 1–250 cm^3/min). The NH_3 conversion (X_{NH_3}) could then be determined from the inlet flow (Q_{in}) of NH_3 and the product flow of $H_2 + N_2$ (Q_{out}) according to Equation (1). A factor of 2 is included in Equation (1) because two moles of NH_3 yield four moles of product (H_2 and N_2) (see Reaction 1). Variations in the measured product flow was used to determine the uncertainty of the conversion.

The energy input normalized H_2 yield was calculated according to Equation (2), where the ratio 3/2 is included due to the stoichiometry of Reaction 1, NH_{3in} is the molar flow rate of NH_3 fed to the reactor, M_{H_2} is the molar mass of hydrogen, and P is the plasma power.

$$X_{NH_3}(\%) = \frac{Q_{out}}{2 \cdot Q_{in}} \cdot 100 \quad (1)$$

$$R_{H_2}\left(\frac{g}{kWh}\right) = \frac{3}{2} \cdot \frac{X_{NH_3} \cdot NH_{3in} \cdot M_{H_2}}{P} \quad (2)$$

The specific energy input (SEI) is defined as the plasma power over the total flow rate (Equation (3)). In addition, we defined an energy efficiency (η_{NH_3}) as the energy required for

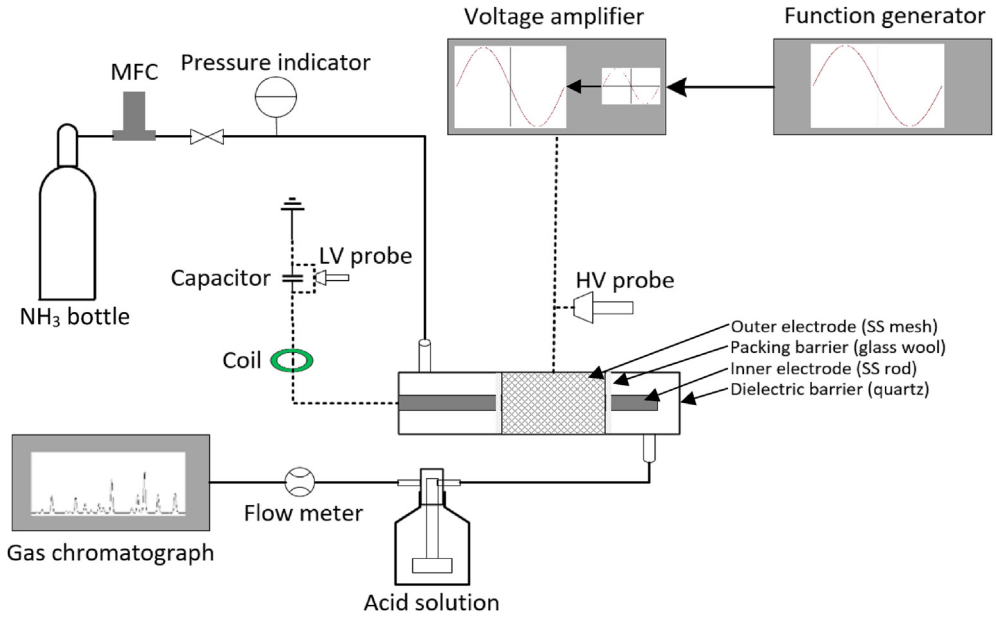

Fig. 2 – Packed-bed DBD reactor with analytical equipment used for NH_3 decomposition.

Reaction 1 relative to the actual energy input, which is calculated from the SEI and the reaction enthalpy ($\Delta_r H$) of the NH_3 decomposition (Equation (4)). A constant SEI of 16.8 J/ml was used for all experiments, except for KM1R and TiO_2 where a value of 12.0 J/ml was used.

$$\text{SEI (J/ml)} = \frac{\text{Plasma power}}{\text{Total feed flow rate}} = \frac{P}{Q_{in}} \quad 3$$

$$\eta_{NH_3}(\%) = \frac{X_{NH_3} \cdot \Delta_r H}{SEI \cdot \rho_{NH_3}/M_{NH_3}} \cdot 100 \quad 4$$

After determining the flow rate, the composition of the product stream was determined by an online gas chromatograph (Thermo Fisher Trace 1300 GC) equipped with a thermal conductivity detector (TCD).

Plasma-catalytic material

Different dielectric materials, commonly used as support materials in thermal catalysis, were tested in this work, including $MgAl_2O_4$ (Haldor Topsoe A/S), HZSM-5 (Si/Al = 25) (Zeolyst CBV5524G), SiO_2 (Saint-Gobain SS 61138), γ-Al_2O_3 (Saint-Gobain SA 6176), m-ZrO_2 (Saint-Gobain SZ 31163), t-ZrO_2/La_2O_3(8.2 wt%) (Saint-Gobain SZ 61156), TiO_2 (Saint-Gobain ST 61120), and $BaTiO_3$ (Sigma Aldrich 1120480250).

The Brunauer-Emmett-Teller (BET) surface area was determined for the mentioned dielectric materials by N_2 physisorption performed at −196 °C (Quantachrome instruments, NOVA touch 2LX). The samples were degassed at 350 °C for 4 h prior to physisorption. Pore volumes were determined by the water uptake of the dried materials (16 h at 120 °C). The measured surface areas and pore volumes are listed in Table 1, along with the relative dielectric constants of the materials.

Experiments were also made using $MgAl_2O_4$ pellets impregnated with different metals. Incipient wetness impregnation was utilized to impregnate the pellets using nitrate salts as the metal precursors, after which the samples were dried and calcined at 450 °C. The resulting materials used were 10 wt% Fe/$MgAl_2O_4$, 10 wt% Ni/$MgAl_2O_4$, 10 wt% Co/$MgAl_2O_4$, and 5 wt%Fe-5 wt.%Ni/$MgAl_2O_4$, which was impregnated in two steps, first iron followed by nickel.

Table 1 – Physicochemical properties of dielectric materials used.

Supports	BET surface area [m^2/g]	Pore volume [cm^3/g]	Median pore diameter [nm]	Relative dielectric constant
HZSM-5	406	0.58	0.5 [24]	3.2 [25]
SiO_2	227	0.77	12[a]	3.9 [26]
$MgAl_2O_4$	23.7	0.28	50[a]	8.3 [27]
γ-Al_2O_3	241	1.04	10[a]	9.0 [26]
m-ZrO_2	51.4	0.28	17[a]	25 [26]
t-ZrO_2/La_2O_3	118	0.27	41[a]	26[b] [26]
TiO_2 (anatase)	139	0.50	16[a]	80 [26]
$BaTiO_3$	3.79	0.07	Not available	1000 [28]

[a] Supplier information.
[b] Determined as a weighted average of the pure oxide components.

Furthermore, an Fe-based commercial NH_3-synthesis catalyst (named KM1R, Haldor Topsoe A/S) was examined. In a standard experiment, the solids were crushed and sieved to a particle size of 0.85–1.4 mm.

Prior to use, the M/$MgAl_2O_4$ (M = Fe, Ni, Co, Fe–Ni) materials were reduced in H_2 at 525 °C for 8 h in a muffle furnace at a flow rate of 300 Nl/min. The samples were then passivated at room temperature with 1% O_2 in N_2 and transferred to the plasma reactor. The samples were then re-reduced before use in a 20 vol% hydrogen/argon plasma with a flow rate of 75 Nml/min for 2 h at a plasma power of 25 W (15 W for KM1R) with a frequency of 3 kHz. Previous work has shown that supported metal oxide catalysts such as Ni/Al_2O_3 can be reduced in a low temperature hydrogen-argon plasma [29,30].

Results and discussion

Electrical characterization

A simplified Q-U Lissajous diagram is shown in Fig. 3, which can provide information about the electrical behavior of the plasma. Four phases, two capacitive phases (AB and CD) and two discharge phases (BC and DA), occurring during one voltage period can be defined on the figure. The capacitive phases represent the periods where the reactor resembles a capacitor and no activity is present in the reaction. In contrast, the discharge phases represent the transformation of the gas volume to a plasma where a net flow of electrons is present. The capacitance of the reactor during a specific phase can be found from Fig. 3 from the related slope, dQ/dU = C [31,32].

Table 2 shows the electrical characterization of the experiments conducted with the dielectric materials. It can be seen that even though the approximately same peak-to-peak voltage (U_{pp}) (see Fig. 3) was recorded, the capacitance of the cell (reactor + gas) (C_{cell}), the effective capacitance (ζ_{diel}), the

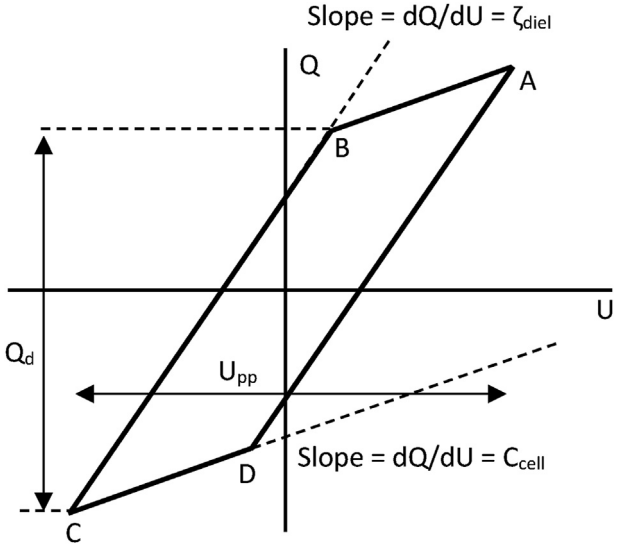

Fig. 3 – Schematic Q-U Lissajous figure indicating typical measured values of the plasma.

Table 2 – Measured data from the oscilloscope and generated Lissajous figures (see Fig. S1 in Supporting Information (SI)) for plasma-only and the dielectric materials.

Packing	U_{pp} (kV)	Plasma power (W)	C_{cell} (pf)	ζ_{diel} (pf)	Q_d (μC)	N_{MD}
None (plasma-only)	22.1	21	7.07	90.59	0.51	21
HZSM-5	22.8	21	38.61	80.62	1.10	5
SiO_2	21.8	21	8.44	74.09	0.52	37
$MgAl_2O_4$	22.2	21	11.20	71.33	0.49	47
γ-Al_2O_3	21.9	21	9.28	73.69	0.52	46
m-ZrO_2	22.1	21	12.07	73.41	0.50	50
t-ZrO_2/La_2O_3	22.5	21	14.27	72.51	0.46	52
TiO_2	22.3	15	43.20	81.31	1.19	4
$BaTiO_3$	22.5	21	39.93	78.93	1.24	4

displaced charges (Q_d), and number of micro-discharges per half period (N_{MD}) changes with the introduced material. Furthermore, the effective capacitance (discharge phase) is observed to be less affected by the dielectric material than the capacitance of the cell (capacitive phases), with the non-packed system yielding the highest effective capacitance and the lowest cell capacitance. HZSM-5, TiO_2, and $BaTiO_3$ differ from the other materials very clearly by having a high cell capacitance, a high number of displaced charges, and a low number of micro-discharges per half period. The number of micro-discharges were determined by examining the current profile (see Fig. 4). In Fig. 4, a positive half period of the current and charge profile is shown. Here, it is observed that the current profiles for HZSM-5, TiO_2, and $BaTiO_3$ show almost no spikes. In contrast to these three materials, the remaining dielectric materials tested and plasma-only showed several (+20) intense current spikes, which is considered to occur due to a micro-discharge. A micro-discharge was therefore counted if the current value increased above the standard deviation. Eight half periods of logged data were used to determine the number of micro-discharges, and N_{MD} is determined as an average per half period over these 8 half periods.

Effect of dielectric material and particle size

After 2 h of operation, the product flow rate was measured over a period of 15 min and the average was used to calculate the conversion according to Equation (1). The resulting conversions obtained from the plasma-assisted ammonia decomposition with the dielectric materials are shown in Fig. 5 with plasma-only as a reference, indicated by the dashed line. Tests with varying flow rate suggest that a higher conversion can be achieved at lower flow rates/longer residence times (Fig. S4). Consequently, the results in Fig. 5 should reflect reaction kinetics and not an equilibrium situation.

A significant increase in the NH_3 conversion compared to plasma-only (5.16%) was achieved when implementing dielectric materials with a relative dielectric constant between 4 and 30 in the plasma zone, with $MgAl_2O_4$ (dielectric constant of 8.3) yielding the highest conversion of 12.6%. Similarly, Wang et al. [20] observed that implementing SiO_2 and Al_2O_3 increased the NH_3 conversion compared to plasma-only. It was further reported by Wang et al. [20] that utilizing packing

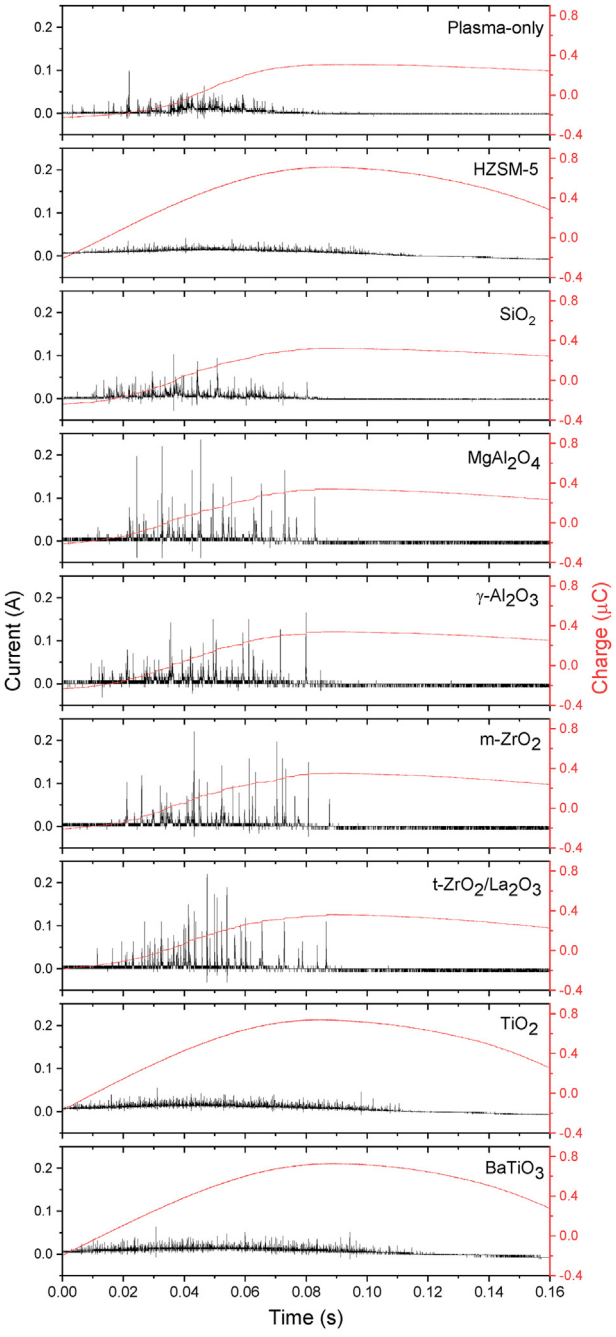

Fig. 4 – Measured current and charge profile for a positive half period.

materials with a higher dielectric constant, such as TiO_2, resulted in a lower NH_3 conversion, which is similar to the results shown in Fig. 5. In the present results, the conversion falls below 1%, i.e. less than for plasma-only, when packing materials with a dielectric constant of 80–1000 are used.

In thermal heterogeneous catalysis, a support material is used to optimize parameters such as surface area, thermal stability, acidity, etc. However, it has previously been shown for other reactions performed in plasma, that implementing different dielectric materials in the plasma zone changes the conversion and electrical characteristics of the system [33,34].

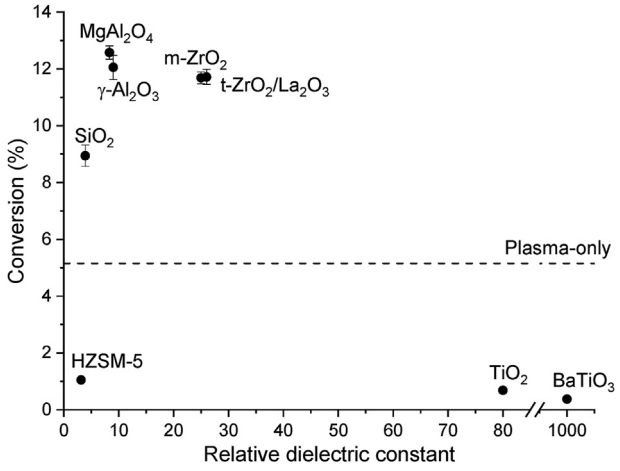

Fig. 5 – NH_3 conversion as function of the relative dielectric constant of different dielectric materials. Results obtained after 2 h in a 21 W (15 W for TiO_2) plasma with a frequency of 3 kHz, discharge gap of 4.5 mm, and flow rate of 75 Nml/min.

Hence, the electrical properties of the support could similarly play an important role in plasma catalysis.

Generally, a decrease in the electron density in the gas phase is observed when utilizing materials with a high dielectric constant in an electric field [28,35]. This is due to accumulation of charges on the surface and loss of electrons to the walls, which is caused by the electric field enhancement at the contact points of these materials and could be a reason for the large decrease in the conversion observed for TiO_2 and $BaTiO_3$ (Fig. 5). This furthermore correlates to the high value of displaced charges observed (Table 2). The high electric field enhancement accelerates the electrons to the surface of the particles, which causes the electrons to lose their capability to move from void to void, hence the plasma is not able to extend from one void to a neighboring void and leads to a shift from a full gap discharge to local discharges [35].

Interestingly, using a material with a very low dielectric constant such as HZSM-5, also results in a reduced conversion and similar electrical measurements as TiO_2 and $BaTiO_3$ (high value of displaced charges and low number of micro-discharges), although such a material with a low dielectric constant should promote a full gap discharge with a low electric field strength [28,35]. When using materials with a relative dielectric constant around 10–20, an optimum in the conversion is achieved. These materials must therefore yield a more optimal balance between the extent of the volume of discharges and the strength of the electric field, which promotes electrons with sufficient energy for breaking an N–H bond (4.5 eV) and stepwise dissociate NH_3, or for excitation to an unstable state that more easily leads to dissociation. This stepwise dissociation through an excited state has been reported for molecules such as CH_4 and CO_2 [36], and is likely the same for NH_3.

From analysis of the Lissajous curves (Fig. S1), it can be observed that the materials showing increased conversion (SiO_2, $MgAl_2O_4$, γ-Al_2O_3, m-ZrO_2, and t-ZrO_2/La_2O_3) promote a lower charge transfer, while also having higher intensity current spikes (Fig. 4). The electrical properties of the materials are thereby shown to be of great importance in plasma catalysis. Furthermore, no significant change in conversion was observed between $MgAl_2O_4$ and γ-Al_2O_3 even though they were found to have different BET surface areas and pore volumes (Table 1), which suggests that surface reactions are unimportant for the enhanced conversion in the presence of these solid packing materials.

The absence of a dependence on surface area (and hence internal porosity within the particles) could be due to the absence of plasma streamers in the pores of the dielectric material. Zhang et al. [37] concluded that the pore size has to be in the order of or bigger than the Debye length for plasma streamers to penetrate into the pores of the structure. For a micro-discharge in a DBD plasma with a spike electron density and temperature of 10^{20} m^{-3} and 20 eV (232000 K) [38], respectively, the Debye length is in the order of 3 μm, which is far greater than the actual pore size of the materials. It is therefore expected that no conversion is occurring in the pores due to the absence of plasma streamers.

The primary role of the solid packing material appears to be in regulating the number of micro-discharges. This is evident from Fig. 6, which shows a correlation between the number of micro-discharges per half period and the NH_3 conversion. Here it is observed that the conversion increases linearly with the number of discharges. Hence, the materials' ability to produce micro-discharges is the central factor for the NH_3 conversion, which to the best of our knowledge have not been reported in literature previously. This suggests that the decomposition reaction occurs in the gas phase and is enabled by the high energy electrons formed during the micro-discharges.

The effect of packing the plasma zone with different particle sizes of $MgAl_2O_4$ on NH_3 conversion is shown in Fig. 7. The conversions show a slightly decreasing trend with increasing particle size. A similar observation was made by El-Shafie et al. [16] where decreasing the particle size from 2 mm to 1 mm also resulted in a slightly higher conversion. However, when taking the experimental uncertainty into account, the statistically significant change is relatively weak.

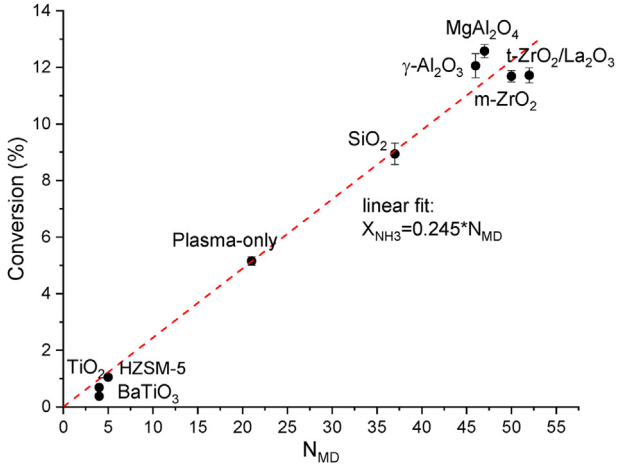

Fig. 6 – NH_3 conversion as function of the number of micro-discharges per half period.

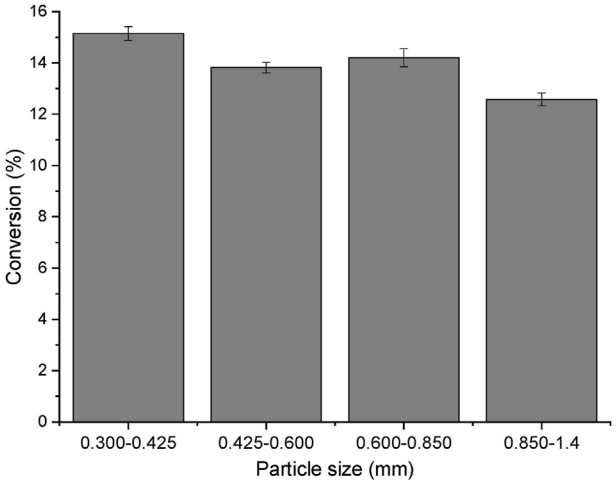

Fig. 7 – NH_3 conversion as function of $MgAl_2O_4$ particle size (21 W, 3 kHz, 4.5 mm gap, and 75 Nml/min). Weight of packing was 10 g for all particle sizes.

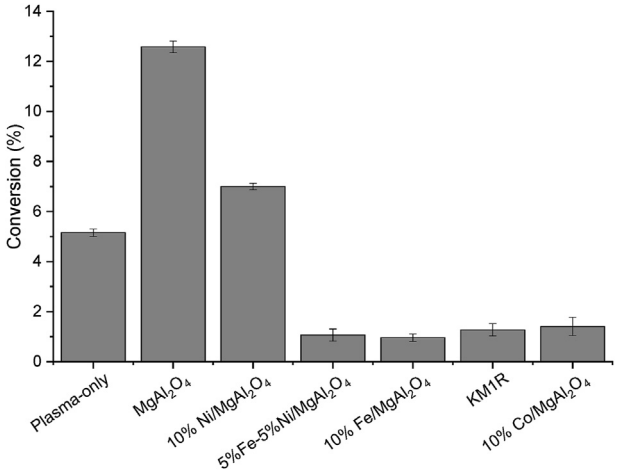

Fig. 8 – Effect of different metal impregnations of $MgAl_2O_4$ on NH_3 conversion (particle size 0.85–1.4 mm, 21 W (15 W for KM1R), 3 kHz, 4.5 mm gap, and 75 Nml/min).

The electrical characterization is found to be similar for the different particle sizes (Table 3), hence no obvious change to the plasma can be found from these data, which is in good agreement with the relatively similar performance. The smaller particle size yields smaller voids between the particles, hence shorter distances for the electrons to jump. This could yield more paths for the electrons to go through the reactor, thereby increasing the probability of an electron-molecule collision, which in turn could increase the conversion. On the other hand, the smaller particle size leads to a weaker electrical field that lowers the energy of the electrons, making the collisions less energetic and thus not capable of breaking or destabilizing the NH_3 molecules [35]. These phenomena seem to largely balance out, leading to the relatively weak size dependence in NH_3 conversion (Fig. 7).

Introduction of metal-containing materials

Impregnating $MgAl_2O_4$ with metals resulted in a decreased conversion relative to the bare support, as shown in Fig. 8. The catalyst containing 10 wt% Ni still showed an improved conversion (7%) compared to the plasma-only, while the catalysts containing Fe, Co, and Fe + Ni showed lower conversions of only ca. 1%. Compared to the finding of Wang et al. [20] and Yi et al. [22], which used similar catalytic metals (Fe, Co, and Ni) and reported conversions above 35%, the observed conversions on Fig. 8 are far lower. However, in both their studies fumed SiO_2 was impregnated with metals and different operating conditions were also used, such as higher SEI.

Interestingly, nickel-containing catalysts have been shown to be effective in other plasma-catalytic systems where production of H_2 is desired such as reforming of hydrocarbons [39,40]. In thermal catalysis, nickel-containing catalysts are used in natural gas steam reforming for H_2 production [41]. Nickel thereby seems to be effective both in thermal catalysis and plasma catalysis when formation of H_2 is desired.

To better understand the influence of the impregnated $MgAl_2O_4$ samples, the electrical parameters of these were analyzed (Fig. S3). It was observed that the catalysts (Fe, Co, and Fe + Ni) with low conversion showed a high charge transfer number and low intensity current spikes, similarly to the dielectric materials providing low conversion (see Figs. 4 and 5). The number of micro-discharges per half cycle was found to be 3, 4, and 5 for Fe–Ni/$MgAl_2O_4$, Fe/$MgAl_2O_4$, and Co/$MgAl_2O_4$, respectively, which all showed conversions of ca. 1%, while Ni (7% conversion) was determined to promote 30 micro-discharges. These results are in good agreement with the trend seen in Fig. 6 (see Supporting Information Fig. S5). Hence the metal-containing solids affect the ammonia conversion by regulating the frequency of micro-discharges in the gas phase rather than through metal-catalyzed surface reactions under the used conditions.

Ideally, a metal is a perfect conductor and therefore has a net electric field inside of zero, which yields a dielectric constant of infinity. This could explain the similar electrical parameters between $TiO_2/BaTiO_3$ and the metal-impregnated $MgAl_2O_4$. However, in contrast to dielectric materials with high dielectric constants, the metals will not have surface charging due to their conductivity [42].

Table 3 – Measured data from the oscilloscope and generated Lissajous figures (Fig. S2) for the different particle sizes of $MgAl_2O_4$.

Particle size (mm)	U_{pp} (kV)	Plasma power (W)	C_{cell} (pf)	ζ_{diel} (pf)	Q_d (μC)	N_{MD}
0.300–0.425	22.0	21	11.06	69.55	0.50	48
0.425–0.600	21.9	21	10.62	71.18	0.54	50
0.600–0.850	21.8	21	10.73	71.15	0.53	54
0.850–1.4	22.2	21	11.20	71.33	0.49	47

Furthermore, the use of an industrial ammonia synthesis catalyst, KM1R, with bulk iron as the primary phase also led to a decrease in the NH_3 conversion. In contrast to the experiments with the impregnated $MgAl_2O_4$, KM1R was only tested at 15 W. Furthermore, the composition of the KM1R also varies from the remaining catalysts, as it mainly consists of iron, while the other metal-containing materials tested mostly consist of a dielectric material (support). This could be the reason why KM1R deviates from the linear relation between conversion and micro-discharge frequency seen for all other experiments (see Fig. S5).

In thermal catalysis, transition metals provide the highest activity for ammonia decomposition since they have the most appropriate nitrogen binding energy [43]. The absence of significant benefits from the transition metals is therefore another indication that the decomposition mainly occurs in the gas phase by interaction with the high energy electrons instead of on the surface of the catalysts.

XRD characterization of catalysts

Fig. 9 shows the XRD patterns of the spent samples measured ex situ. The primary contribution to the diffraction pattern comes from the $MgAl_2O_4$ support, which shows indications of both $MgAl_2O_4$, and Al_2O_3 phases that are also seen in M/$MgAl_2O_4$ (M = Co, Fe, Fe–Ni, and Ni) samples. The XRD pattern of the spent Co/$MgAl_2O_4$ sample shows two weak reflection peaks at 43.8° and 51.1° that correspond to metallic Co, and the spent Ni/$MgAl_2O_4$ sample shows reflections at 44.5°and 51.9° indicating metallic Ni. For Fe/$MgAl_2O_4$ a reflection is present at 44.7°, which is consistent with metallic Fe. These samples thus verifiably contained metallic particles during the reaction, since metallic phases are even preserved in these ex situ analyses. If metal-catalyzed surface reactions were important in the plasma-assisted ammonia decomposition, these samples should thus have caused an effect. The diffraction pattern for the spent Fe–Ni/$MgAl_2O_4$ sample does not differ strongly from the support. Hence, Fe and Ni must be present as either very small metal nanoparticles or as amorphous oxide phases, but given the ex situ nature of the analyses it is difficult to establish if metallic or oxidized phases dominated under reaction conditions.

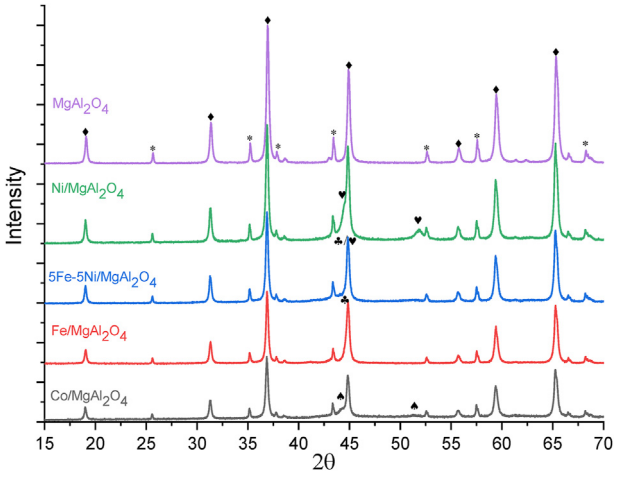

Fig. 9 – XRD pattern of spent catalytic material (◆$MgAl_2O_3$, *Al_2O_3, ♥Ni, ♣Fe, and ♠Co).

Effect of insulating the reactor

A second set of NH_3 decomposition experiments was conducted with the same catalytic materials, where the reactor was insulated with woven ceramic fibers, hence no repacking was conducted between the first and second set of experiments with a specific packing material. The resulting temperatures with the insulation material tightly wrapped around the reactor are shown in Table 4. The temperatures were measured on the outside of the reactor wall with a thermocouple placed between the reactor and the insulation material, immediately after turning off the plasma. It can be seen that insulating the reactor increases the reactor temperature by approximately 100 °C. The effect on NH_3 conversion of insulating the reactor is shown on Fig. 10.

A negative effect on the conversion is observed when adding the insulation for the modes with a conversion above 2%, with plasma-only decreasing from 5.0% to 4.4%, $MgAl_2O_4$ from 12.6% to 9.9%, and Ni from 7.0% to 5.9%. For the remaining catalysts, the effect was within the experimental uncertainty. In spite of the increased activity that comes from the rise in temperature, the gas temperature is still too low for a thermal effect with the catalysts tested, even though the equilibrium prescribes a 90% conversion at 225 °C. Wang et al. [18] observed a large decrease in NH_3 conversion (from ca. 95%–12%) when the temperature was decreased from 400 °C to 300 °C when using Co/fumed SiO_2. A similar observation was reported in another study by Wang et al. [19] where an Fe catalyst was used. Here, the plasma alone succeeded the NH_3 conversion of the plasma + Fe catalyst at 300 °C. Furthermore, Yi et al. [22] also reported a decrease in NH_3 conversion for a Fe–Ni catalyst (from ca. 30%–11%) when decreasing the temperature from 400 °C to 340 °C. These observations correlate with the low conversions observed on Fig. 10 where a maximum temperature of 245 °C was achieved, indicating that the surface reactions are not yet sufficiently fast at the achieved temperatures.

The number of micro-discharges was not affected by the temperature increase. However, the increase in gas temperature that comes from insulating the reactor, increases the volumetric flow rate and lowers the residence time of the gas in the plasma zone, which in turn lowers the probability of an electron-molecule collision. This change in gas residence time within the plasma zone is therefore the most likely reason for the lowered NH_3 conversion. This is in agreement with the observation of a declining conversion with increasing residence time when the residence time was altered through the feed flow rate (see Fig. S4).

It is worth noting, that a lower applied voltage was needed to reach the plasma power of 21 W when insulation was placed around the reactor. This gives a weaker electrical field, thereby causing the plasma to deliver a lower acceleration of the electrons, but the same energy per time. A lower energy transfer is therefore expected in the electron-molecule collisions, which in turn leads to fewer collision induced reaction events. Several parameters could therefore have caused the decrease in conversion.

Table 4 – Measured temperatures on the outside of the reactor.

	Plasma-only	$MgAl_2O_4$	$Ni/MgAl_2O_4$	$Fe–Ni/MgAl_2O_4$	$Fe/MgAl_2O_4$	$Co/MgAl_2O_4$	KM1R
T (no insulation)	135 °C	130 °C	135 °C	140 °C	135 °C	135 °C	95 °C
T (with insulation)	235 °C	235 °C	225 °C	245 °C	250 °C	225 °C	200 °C

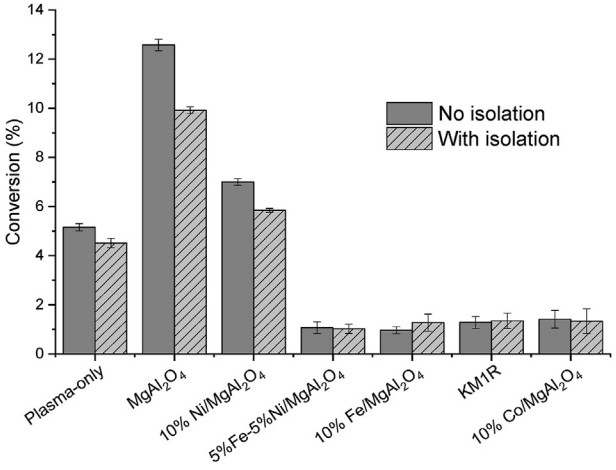

Fig. 10 – Effect of different impregnations on NH_3 conversion and insulating the reactor (21 W (15 W for KM1R), 3 kHz, 4.5 mm gap, and 75 Nml/min).

Hydrogen formation rate and energy efficiency

From the gas chromatograph measurements, it was determined that the product flow from the experiments with a conversion above 2% contained a H_2:N_2 fraction of 3:1 as prescribed by Reaction 1, with no NH_3 remaining after the absorption in sulfuric acid. The experiments with a conversion below 2% produced too low flow rates after absorption for accurate measurements on the gas chromatograph, hence a H_2:N_2 fraction of 3:1 could not be determined, but still some H_2 was detected. The "make up" gas in these small samples was air, as an increased content of N_2 was detected, along with an impurity of O_2. Hydrazine has been reported as a by-product from studies diluting NH_3 with Ar [7,44], but not from studies using pure NH_3 [18–22] or dilution with N_2 [15]. In this work, pure NH_3 was converted into H_2 and no hydrazine was detected on the GC measurements. However, the hydrazine would also have been removed as the product stream was bubbled through the acidic solution.

The calculated energy input normalized H_2 yields (R_{H_2}) of selected packing materials are shown in Table 5, along with the energy efficiency and conversion. As expected from Equations (2) and (4), the H_2 yield and energy efficiency increase with conversion, giving that using $MgAl_2O_4$ with a particle size of 0.300–0.425 mm for NH_3 decomposition results in the highest energy input normalized H_2 yield (4.08 g/kWh) and energy efficiency (1.73%). For comparison, the theoretical value of R_{H_2} based on the reaction enthalpy is 235 g/kWh.

To our knowledge, only few publications have investigated plasma-catalytic ammonia decomposition [15–23]. Interestingly, a hydrogen formation rate of 32 g/kWh (98% NH_3 conversion) was reported by Wang et al. [18], i.e. about 10 times higher than reported in this study. However, this was at a measured reaction temperature of 380 °C generated by the plasma and substantial thermal conversion must also have contributed. A lower flow rate, smaller plasma volume, and higher power input could be the reason for the higher temperature and NH_3 conversion achieved by Wang et al. [18], which resembles the parameters also used in Refs. [19–21].

Table 5 – H_2 formation rate and energy efficiency for selected packing materials.

Packing	Conversion [%]	R_{H_2} [g/kWh]	η [%]
Non (Plasma-only)	5.16	1.36	0.58
SiO_2	8.94	2.41	1.02
$MgAl_2O_4$ (0.300–0.425 mm)	15.1	4.08	1.73
γ-Al_2O_3	12.1	3.25	1.38
m-ZrO_2	11.7	3.15	1.33
$Ni/MgAl_2O_4$	7.00	1.89	0.80

Conclusion

It has been shown that a plasma is able to decompose NH_3 at atmospheric pressure and with no external heating and produce clean hydrogen from sustainable power. A decomposition of 5% NH_3 for plasma-only was achieved at the applied conditions. The effect of applying a packing material (pure dielectric material or impregnated with metal) in the plasma zone was tested. In general, dielectric materials with a relative dielectric constant in the range 10–30 were found to give strong synergies with the plasma, leading to enhanced NH_3 conversion. Interestingly, an optimum in the conversion was found when utilizing materials with a relative dielectric constant around 10 and implementing $MgAl_2O_3$ (dielectric constant of 8.3) in the plasma zone increased the conversion by a factor of ca. 2.5, to 12.6%. Furthermore, the effect of particle size of $MgAl_2O_4$ was found to have only minor influence on the NH_3 conversion, with a maximum of 15.1% achieved with a particle size of 300–425 μm.

Impregnating $MgAl_2O_4$ with metals (Fe, Ni, Fe–Ni, and Co) was found to decrease the conversion due to the fast removal of electrons caused by the metals' high conductivity and significantly lower number of formed micro-discharges. When insulating the reactor, causing a temperature increase of ca. 100 °C, a decrease in conversion was observed because of a decreased residence time of the gas, without observations of an enhancement in thermally induced conversion.

In addition, there was found a linear correlation between the number of micro-discharges and the conversion, which indicates that the decomposition of NH_3 in plasma primarily proceeds in the gas phase by collision with high-energy electrons. Furthermore, the packing materials were observed to mainly alter the plasma parameters when the temperature is

too low for a thermo-catalytic effect. The number of micro-discharges per half period is therefore a key parameter in NH_3 decomposition.

Declaration of competing interest

The authors declare that they have no known competing financial interests or personal relationships that could have appeared to influence the work reported in this paper.

Acknowledgment

We thank Haldor Topsoe A/S and Saint-Gobain for providing the catalytic materials and the Department of Chemical and Biochemical Engineering, Technical University of Denmark, for funding this project.

Appendix A. Supplementary data

Supplementary data to this article can be found online at https://doi.org/10.1016/j.ijhydene.2022.07.102.

REFERENCES

[1] Bell TE, Torrente-Murciano L. H_2 production via ammonia decomposition using non-noble metal catalysts: a review. Top Catal 2016;59:1438–57. https://doi.org/10.1007/s11244-016-0653-4.
[2] Schüth F, Palkovits R, Schlögl R, Su DS. Ammonia as a possible element in an energy infrastructure: catalysts for ammonia decomposition. Energy Environ Sci 2012;5:6278–89. https://doi.org/10.1039/c2ee02865d.
[3] Chellappa AS, Fischer CM, Thomson WJ. Ammonia decomposition kinetics over Ni-Pt/Al_2O_3 for PEM fuel cell applications. Appl Catal Gen 2002;227:231–40. https://doi.org/10.1016/s0926-860x(01)00941-3.
[4] Lamb KE, Dolan MD, Kennedy DF. Ammonia for hydrogen storage; A review of catalytic ammonia decomposition and hydrogen separation and purification. Int J Hydrogen Energy 2019;44:3580–93. https://doi.org/10.1016/j.ijhydene.2018.12.024.
[5] Mukherjee S, Devaguptapu SV, Sviripa A, Lund CRF. Low-temperature ammonia decomposition catalysts for hydrogen generation. Appl Catal B Environ 2018;226:162–81. https://doi.org/10.1016/j.apcatb.2017.12.039.
[6] Yin SF, Xu BQ, Zhou XP, Au CT. A mini-review on ammonia decomposition catalysts for on-site generation of hydrogen for fuel cell applications. Appl Catal Gen 2004;277:1–9. https://doi.org/10.1016/j.apcata.2004.09.020.
[7] Fateev A, Leipold F, Kusano Y, Stenum B, Tsakadze E, Bindslev H. Plasma chemistry in an atmospheric pressure Ar/NH_3 dielectric barrier discharge. Plasma Process Polym 2005;2:193–200. https://doi.org/10.1002/ppap.200400051.
[8] Lendzion-Bielun Z, Narkiewicz U, Arabczyk W. Cobalt-based catalysts for ammonia decomposition. Materials 2013;6:2400–9. https://doi.org/10.3390/ma6062400.
[9] Feyen M, Weidenthaler C, Güttel R, Schlichte K, Holle U, Lu AH, et al. High-temperature stable, iron-based core-shell catalysts for ammonia decomposition. Chem Eur J 2011;17:598–605. https://doi.org/10.1002/chem.201001827.
[10] Simonsen SB, Chakraborty D, Chorkendorff I, Dahl S. Alloyed Ni-Fe nanoparticles as catalysts for NH_3 decomposition. Appl Catal Gen 2012;447–448:22–31. https://doi.org/10.1016/j.apcata.2012.08.045.
[11] Zheng W, Zhang J, Ge Q, Xu H, Li W. Effects of CeO_2 addition on Ni/Al_2O_3 catalysts for the reaction of ammonia decomposition to hydrogen. Appl Catal B Environ 2008;80:98–105. https://doi.org/10.1016/j.apcatb.2007.11.008.
[12] Choudhary TV, Sivadinarayana C, Goodman DW. Catalytic ammonia decomposition: COx-free hydrogen production for fuel cell applications. Catal Lett 2001;72:197–201.
[13] Li XK, Ji WJ, Zhao J, Wang SJ, Au CT. Ammonia decomposition over Ru and Ni catalysts supported on fumed SiO_2, MCM-41, and SBA-15. J Catal 2005;236:181–9. https://doi.org/10.1016/j.jcat.2005.09.030.
[14] Silva Hugo, Nielsen Morten G, Fiordaliso Elisabetta M, Damsgaard Christian D, Gundlach Carsten, Kasama Takeshi, et al. Synthesis and characterization of Fe–Ni/ɣ-Al_2O_3 egg-shell catalyst for H_2 generation by ammonia decomposition. Appl Catal Gen 2015;505:548–56.
[15] Akiyama M, Aihara K, Sawaguchi T, Matsukata M, Iwamoto M. Ammonia decomposition to clean hydrogen using non-thermal atmospheric-pressure plasma. Int J Hydrogen Energy 2018;43:14493–7. https://doi.org/10.1016/j.ijhydene.2018.06.022.
[16] El-Shafie M, Kambara S, Hayakawa Y. Alumina particle size effect on H_2 production from ammonia decomposition by DBD plasma. Energy Rep 2020;6:25–30. https://doi.org/10.1016/j.egyr.2020.10.032.
[17] El-Shafie M, Kambara S, Hayakawa Y. Plasma-enhanced catalytic ammonia decomposition over ruthenium (Ru/Al_2O_3) and soda glass (SiO_2) materials. J Energy Inst 2021;99:145–53. https://doi.org/10.1016/j.joei.2021.09.001.
[18] Wang L, Yi Y, Guo HC, Du XM, Zhu B, Zhu YM. Highly dispersed co nanoparticles prepared by an improved method for plasma-driven NH_3 decomposition to produce H_2. Catalysts 2019;9:1–13. https://doi.org/10.3390/catal9020107.
[19] Wang L, Yi Y, Guo Y, Zhao Y, Zhang J, Guo H. Synergy of DBD plasma and Fe-based catalyst in NH_3 decomposition: plasma enhancing adsorption step. Plasma Process Polym 2017;14:1600111. https://doi.org/10.1002/ppap.201600111.
[20] Wang L, Yi Y, Zhao Y, Zhang R, Zhang J, Guo H. NH_3 decomposition for H_2 generation: effects of cheap metals and supports on plasma-catalyst synergy. ACS Catal 2015;5:4167–74. https://doi.org/10.1021/acscatal.5b00728.
[21] Wang L, Zhao Y, Liu C, Gong W, Guo H. Plasma driven ammonia decomposition on a Fe-catalyst: eliminating surface nitrogen poisoning. Chem Commun 2013;49:3787–9. https://doi.org/10.1039/c3cc41301b.
[22] Yi Y, Wang L, Guo Y, Sun S, Guo H. Plasma-assisted ammonia decomposition over Fe–Ni alloy catalysts for COx-Free hydrogen. AIChE J 2019;65:691–701. https://doi.org/10.1002/aic.16479.
[23] Hayakawa Y, Kambara S, Miura T. Hydrogen production from ammonia by the plasma membrane reactor | Elsevier Enhanced Reader. Int J Hydrogen Energy 2020;45:32082–8. https://doi.org/10.1016/j.ijhydene.2020.08.178.
[24] Eschenbacher A, Afzali Andersen J, Degn Jensen A. Catalytic conversion of acetol over HZSM-5 catalysts-influence of Si/Al ratio and introduction of mesoporosity. Catal Today 2021;365:301–9. https://doi.org/10.1016/j.cattod.2020.03.041.
[25] Dietrich M, Rauch D, Simon U, Porch A, Moos R. Ammonia storage studies on H-ZSM-5 zeolites by microwave cavity perturbation: correlation of dielectric properties with

ammonia storage. J Sens Sens Syst 2015;4:263–9. https://doi.org/10.5194/jsss-4-263-2015.
[26] Robertson A. High dielectric constant oxides. Eur Phys J Appl Phys 2004;28:265–91. https://doi.org/10.1051/epjap.
[27] Shannon RD, Rossman GR. Dielectric constant of $MgAl_2O_4$ spinel and the oxide additivity rule. J Phys Chem Solid 1991;52:1055–9.
[28] Van Laer K, Bogaerts A. Influence of gap size and dielectric constant of the packing material on the plasma behaviour in a packed bed DBD reactor: a fluid modelling study. Plasma Process Polym 2017;14:1600129. https://doi.org/10.1002/ppap.201600129.
[29] Tu X, Gallon HJ, Whitehead JC. Plasma-assisted reduction of a NiO/Al_2O_3 catalyst in atmospheric pressure H_2/Ar dielectric barrier discharge. Catal Today 2013;211:120–5.
[30] Andersen JA, Christensen JM, Østberg M, Bogaerts A, Jensen AD. Plasma-catalytic dry reforming of methane: screening of catalytic materials in a coaxial packed-bed DBD reactor. Chem Eng J 2020;397. https://doi.org/10.1016/j.cej.2020.125519.
[31] Manley TC. The electric characteristics of the ozonator discharge. J Electrochem Soc 1943;84:83–96. https://doi.org/10.1149/1.3071556.
[32] Peeters FJJ, van de Sanden MCM. The influence of partial surface discharging on the electrical characterization of DBDs. Plasma Sources Sci Technol 2015;24. https://doi.org/10.1088/0963-0252/24/1/015016. 015016.
[33] Michielsen I, Uytdenhouwen Y, Bogaerts A, Meynen V. Altering conversion and product selectivity of dry reforming of methane in a dielectric barrier discharge by changing the dielectric packing. Mater Catal 2019;9:51. https://doi.org/10.3390/catal9010051.
[34] Uytdenhouwen Y, Van Alphen S, Michielsen I, Meynen V, Cool P, Bogaerts A. A packed-bed DBD micro plasma reactor for CO_2 dissociation: does size matter? Chem Eng J 2018;348:557–68. https://doi.org/10.1016/j.cej.2018.04.210.
[35] Van Laer K, Bogaerts A. How bead size and dielectric constant affect the plasma behaviour in a packed bed plasma reactor: a modelling study. Plasma Sources Sci Technol 2017;26. https://doi.org/10.1088/1361-6595/aa7c59.
[36] Chung W-C, Chang M-B. Review of catalysis and plasma performance on dry reforming of CH_4 and possible synergistic effects. Renew Sustain Energy Rev 2016;62:13–31. https://doi.org/10.1016/j.rser.2016.04.007.
[37] Zhang Q-Z, Bogaerts A. Propagation of a plasma streamer in catalyst pores. Plasma Sources Sci Technol 2018;27. https://doi.org/10.1088/1361-6595/aab47a. 035009.
[38] van 't Veer K, Engelmann Y, Reniers F, Bogaerts A. Plasma-catalytic ammonia synthesis in a DBD plasma: role of microdischarges and their afterglows. J Phys Chem C 2020;124:22871–83. https://doi.org/10.1021/acs.jpcc.0c05110.
[39] Wu J, Xia Q, Wang H, Li Z. Catalytic performance of plasma catalysis system with nickel oxide catalysts on different supports for toluene removal: effect of water vapor. Appl Catal B Environ 2014;156–157:265–72. https://doi.org/10.1016/j.apcatb.2014.03.017.
[40] Zeng Y, Zhu X, Mei D, Ashford B, Tu X. Plasma-catalytic dry reforming of methane over y-Al_2O_3 supported metal catalysts. Catal Today 2015;256:80–7. https://doi.org/10.1016/j.cattod.2015.02.007.
[41] Mortensen PM, Dybkjær I. Industrial scale experience on steam reforming of CO_2-rich gas. Appl Catal Gen 2015;495:141–51. https://doi.org/10.1016/j.apcata.2015.02.022.
[42] Zhang Q-Z, Bogaerts A. Importance of surface charging during plasma streamer propagation in catalyst pores. Plasma Sources Sci Technol 2018;27:65009. https://doi.org/10.1088/1361-6595/aaca6d.
[43] Aika K-I, Yamaguchi J, Ozaki A. Ammonia synthesis over rhodium, iridium and platinum promoted by potassium. Chem Lett 1973;2:161–4.
[44] Sakai O, Hiraoka Y, Kihara N, Blanquet E, Urabe K, Tanaka M. Microdischarge-induced decomposition of ammonia and reduction of silver ions for formation of two-dimensional network structure. Plasma Chem Plasma Process 2016;36:281–94. https://doi.org/10.1007/s11090-015-9664-3.